AUTONOMOUS VEHICLES

Liquid-amplified zipping actuators for micro-air vehicles with transmission-free flapping

Tim Helps[1,2], Christian Romero[1,2,3,4], Majid Taghavi[1,2], Andrew T. Conn[2,5], Jonathan Rossiter[1,2]*

Flapping micro-air vehicles (MAVs) can access a wide range of locations, including confined spaces such as the inside of industrial plants and collapsed buildings, and offer high maneuverability and tolerance to disturbances. However, current flapping MAVs require transmission systems between their actuators and wings, which introduce energetic losses and additional mass, hindering performance. Here, we introduce a high-performance electrostatic flapping actuation system, the liquid-amplified zipping actuator (LAZA), which induces wing movement by direct application of liquid-amplified electrostatic forces at the wing root, eliminating the requirement of any transmission system and their associated downsides. The LAZA allows for accurate control of flapping frequency and amplitude, exhibits no variation in performance over more than 1 million actuation cycles, and delivers peak and average specific powers of 200 and 124 watts per kilogram, respectively, exceeding mammalian and insect flight muscle and on par with modern flapping MAV actuation systems. The inclusion of 50-millimeter-long passively pitching wings in a dragonfly-sized LAZA flapping system allowed the rectification of net directional thrust up to 5.73 millinewtons. This thrust was achieved while consuming only 243 milliwatts of electrical power, implying a thrust-to-power ratio of 23.6 newtons per kilowatt, similar to state-of-the-art flapping MAVs, helicopter rotors, and commercial drone motors. Last, a horizontally moving LAZA flapping system supported by a taut nylon wire was able to accelerate from at-rest and travel at speeds up to 0.71 meters per second. The LAZA enables lightweight, high-performance transmission-free flapping MAVs for long-term remote exploration and search-and-rescue missions.

INTRODUCTION

The vast majority of vehicles use wheels for locomotion, yet only around half of Earth's landmass is accessible to wheeled and tracked systems (*1*). In contrast, devices that fly can reach almost all locations. Micro-air vehicles (MAVs) allow access to an even wider range of locales, promising aerial exploration of confined spaces such as the interiors of buildings (*2*, *3*) and more effective search-and-rescue functionality. Flapping MAVs, which operate using the reciprocating motion of wings rather than the rotating propellers typical in commercial drones, offer improved maneuverability, gust tolerance, and disturbance rejection (*4*) and the potential for quieter flight (*5*).

Flapping MAVs generate the reciprocating motion of their wings by exerting time-varying forces at the wing root. Various combinations of actuation technology and transmission system have been demonstrated to achieve these cyclic forces. Most commonly, electric motors are used, combined with transmission systems that convert rotary to oscillatory motion such as string-based mechanisms (*6*), four-bar mechanisms with sliders (*7*, *8*), gear boxes (*9*), and combined four-bar linkage and pulley-string systems (*10*). More unusual combinations included servo motors and an "elaborate" gearbox (*11*) and piezoelectric bending cantilevers with flexure-based transmissions (*12*). Recently, effective electrostatic systems have been demonstrated, including a double-cone dielectric elastomer actuator (DEA) system with a double rocker and slider crank mechanism (*13*) and flapping MAVs driven by cylindrically rolled DEAs and four-bar transmissions (*14*).

A fundamental limitation on the performance of MAVs is their total mass, which directly influences acceleration and maneuverability. The actuator and transmission constitute a major contributor to system mass, comprising 27 to 49% of total system mass (*6*–*8*, *10*, *12*); the flapping mechanism and structure alone can account for up to 27.1% of total flapping MAV mass (*8*). Furthermore, the transmission system introduces frictional or viscous losses, which reduce the overall effectiveness of the flapping system, and transmission systems with cranks or levers can also introduce unwanted varying transmission ratios.

Here, we introduce an actuation system for flapping, the liquid-amplified zipping actuator (LAZA), which enables transmission-free flapping MAVs (Fig. 1A and Movie 1). To induce wing movement, time-varying electrostatic forces are exerted directly at the wing root. The actuation system to generate these forces comprises only simple insulated electrodes that form part of the chassis and wing (Fig. 1B). These electrodes can be extremely thin and lightweight, and there is no requirement of any transmission system or flapping mechanism whatsoever, completely eliminating the mass, inefficiency, and varying transmission ratio associated with these systems.

The LAZA takes advantage of the principle of liquid-amplified electrostatic zipping (*15*) whereby electrostatic forces are concentrated at a single, moving zipping point, thereby delivering strong and incremental actuation. These devices have been shown to exhibit high static (contraction exceeding 99%; specific energy, 6.88 J kg^{-1}) and dynamic performance (average contraction rate, 1161% s^{-1}; average specific power, 51.45 W kg^{-1}) (*15*). Here, we extend their performance for high-speed actuation, which enables fast resonant drive of flapping MAVs. In the LAZA, the application of high voltage between the insulated top or bottom chassis electrode and the wing electrode induces an electrostatic attractive force, which is coupled to Maxwell pressure, $P \propto \varepsilon_0 \varepsilon_r E^2$, where ε_0 is the vacuum permittivity, ε_r is the relative permittivity of the medium between the electrodes,

[1]Department of Engineering Mathematics, University of Bristol, Bristol, UK. [2]Bristol Robotics Laboratory, University of Bristol, Bristol, UK. [3]Bristol Centre for Functional Nanomaterials, School of Physics, University of Bristol, Bristol, UK. [4]School of Chemistry, University of Bristol, Bristol, UK. [5]Department of Mechanical Engineering, University of Bristol, Bristol, UK.
*Corresponding author. Email: jonathan.rossiter@bristol.ac.uk

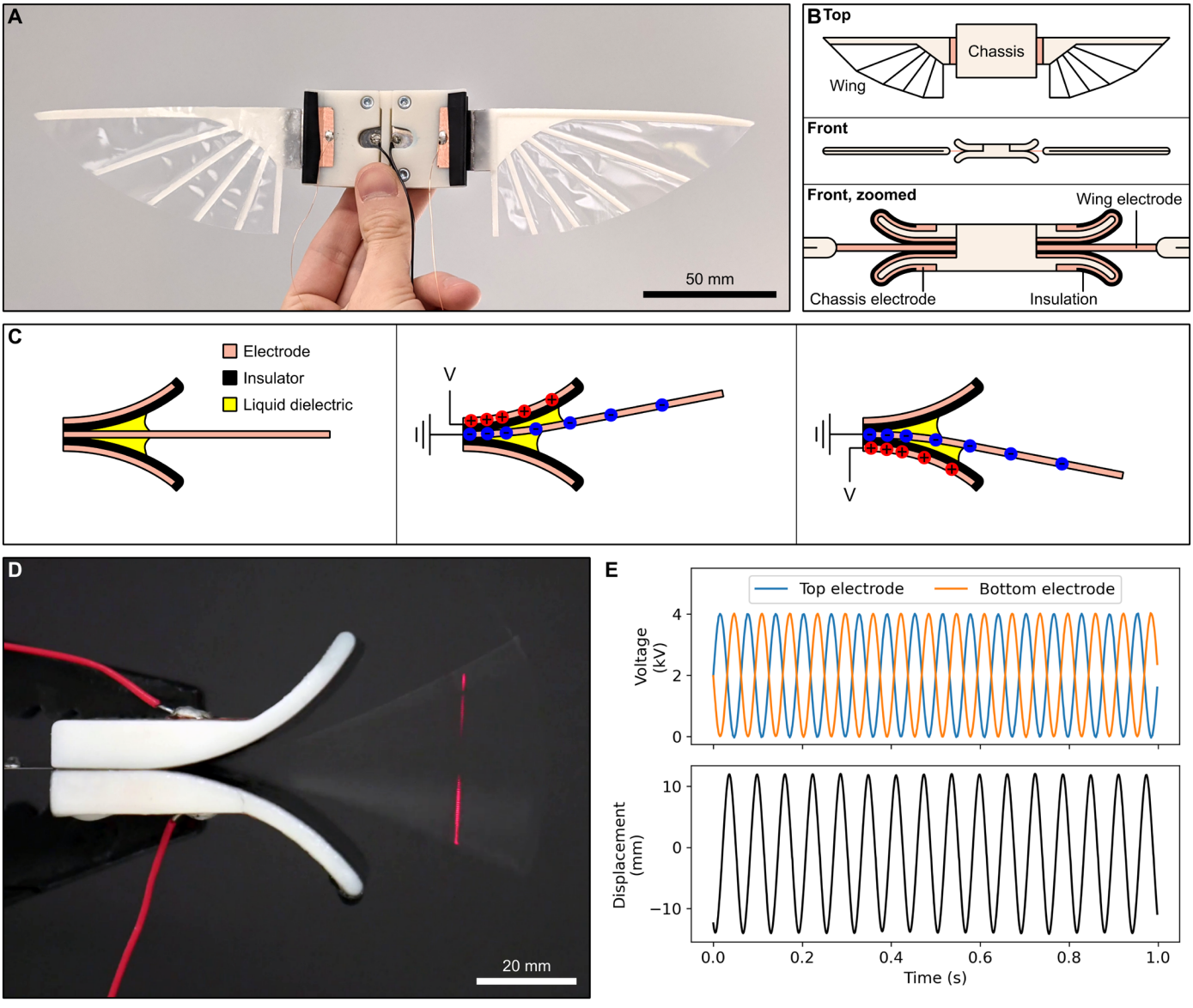

Fig. 1. Transmission-free flapping MAVs. (**A**) Photo of an example transmission-free flapping MAV prototype. (**B**) Top, front, and zoomed front views of proposed transmission-free flapping MAV design. (**C**) Actuation principle of the LAZA, which exerts time-varying electrostatic forces on the wing electrode to induce wing movement. Movie 2 shows the principle in action. (**D**) Photograph of LAZA during testing, showing wing electrode oscillation at 23 Hz. The laser beam used to measure amplitude is visible. (**E**) Time-varying voltage applied to the top and bottom electrode, and resultant movement of the central electrode. Maximum voltage V_{max} = 4 kV.

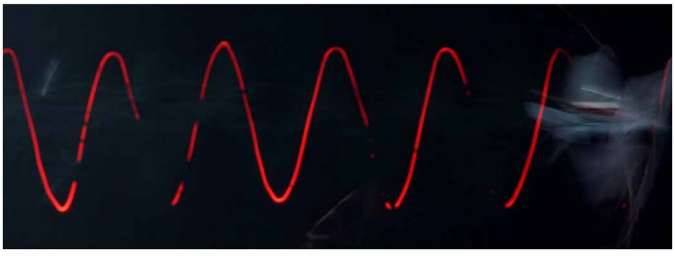

Movie 1. LAZAs for MAVs with transmission-free flapping.

and E is the electric field (*16*). If the medium between the electrodes is air, its relative permittivity is about 1, and the electric field is limited by the dielectric strength E_{max} of air, about 3 MV m^{-1}. This constrains the electrostatic force, making it too small to induce useful movement. To overcome this issue, a small droplet (around 0.4 ml) of liquid dielectric (silicone oil) is added, increasing the permittivity and dielectric strength of the medium and considerably amplifying electrostatic force: relative permittivity ε_r is increased from 1 to 2.7, and dielectric strength E_{max} is increased from 3 to 20 MV m^{-1}. This increases Maxwell pressure $P \propto \varepsilon_0 \varepsilon_r E^2$ up to 120-fold compared with a system lacking any liquid dielectric. Taghavi *et al.* (*15*) provide a full description of the factors influencing electrostatic force for liquid-amplified electrostatic actuators

$$F = \frac{\frac{1}{2}\varepsilon_{medium}\varepsilon_0 A V^2}{\left(\frac{\varepsilon_{medium}}{\varepsilon_{insulator}} t_{insulator} + t_{medium}\right)^2} \quad (1)$$

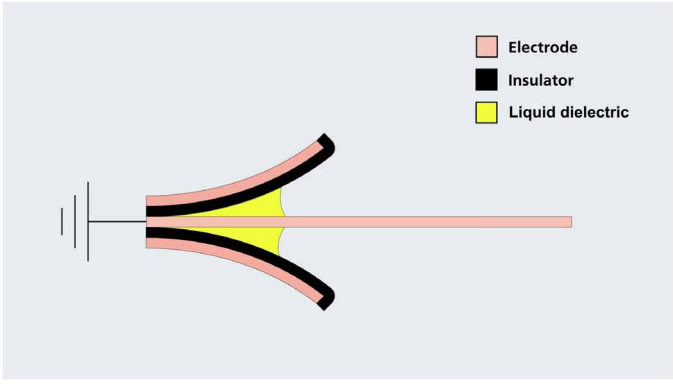

Movie 2. LAZA principle. The application of high voltage induces electrostatic attraction between electrodes, resulting in controllable flapping movement of the wing electrode.

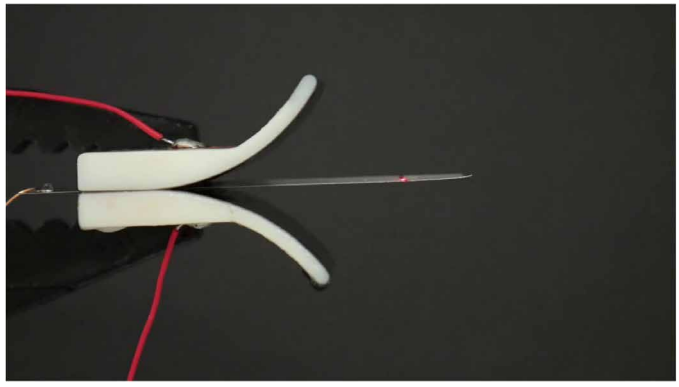

Movie 3. LAZA in action. A LAZA actuates a 70-μm-thick wing electrode at a maximum voltage of 7 kV and a frequency of 23 Hz. A 1/16× slow-motion video of the same LAZA system is subsequently shown, recorded at 240 FPS.

where F is the electrostatic force; ε_{medium} and $\varepsilon_{insulator}$ are the permittivity of the medium and insulator, respectively; A is the area of the electrodes; V is the applied voltage; and $t_{insulator}$ and t_{medium} are the insulator and medium thickness, respectively. If the insulator is thin compared with the medium, the attractive force reduces to Maxwell pressure. This model does not include the effect of adhesive, cohesive, wetting, or capillary forces associated with the droplet of liquid dielectric; these are assumed to be negligible here, due to the extremely low viscosity of the liquid dielectric used.

As has been shown, the droplet of liquid dielectric has a strong influence upon the performance of systems that take advantage of liquid-amplified electrostatic zipping, and loss of the droplet could result in a considerable reduction in performance. Conveniently, the droplet is retained in its location by dielectrophoretic forces, which are also induced by the electric field and act to draw high-permittivity materials toward areas of high electric field density (*17*, *18*).

To induce oscillatory movement of the wing, we apply a time-varying voltage profile to the chassis electrodes with respect to the wing electrode (Fig. 1C and Movie 2). Any arbitrary voltage profile can be applied; however, initial investigations showed that sinusoidal variations in voltage maximized the flapping amplitude. The sinusoidal voltage profiles are 180° out of phase with one another such that, when the wing electrode is maximally attracted toward one chassis electrode, it experiences no attractive force toward the other. These combined forces induce smooth oscillatory movement of the wing electrode (Fig. 1, D and E, and Movie 3). This contrasts with traditional flapping MAVs that feature transmission systems, where nonsmooth dynamics can be introduced by varying transmission ratios and reflected inertia. The wing electrode's motion is almost entirely oscillatory, resembling a vibrating beam oscillating in its first mode of vibration.

Once oscillatory wing movement has been attained, pitching wings that allow the rectification of net directional thrust during flapping can be included. This allows the LAZA to provide acceleration and high-speed forward movement in a transmission-free flapping MAV, with none of the mass and inefficiency associated with the traditional actuator and transmission system. The LAZA and the transmission-free flapping MAV concept enables a class of simple, reliable, lightweight, high-performance MAVs suitable for future aerial exploration applications.

RESULTS

LAZA behavior

The LAZA comprises a pair of insulated chassis electrodes, a wing electrode (which is moved by electrostatic forces), and a small droplet of liquid dielectric. In the absence of any liquid dielectric, flapping performance was poor, and electric breakdown became increasingly likely as applied voltage was increased (Fig. 2, A and B). Performance is affected by material properties, system dimensions, and electrical parameters. Predictably, the viscosity of the liquid dielectric has a strong influence on flapping amplitude, with more viscous liquids inducing more viscous damping, reducing performance (Fig. 2B). In all subsequent experiments, the lowest viscosity liquid dielectric is used: 5 cSt silicone oil (317667, Sigma-Aldrich). Hence, in the subsequent LAZA systems described here, the fluidic effects of the droplet of liquid dielectric—such as adhesion, wetting, capillary forces, and viscosity—are assumed to be negligible and are incorporated into the general effects contributing to energy loss in the oscillating wing electrode.

The wing electrode behaves as a flexural cantilever beam, exerting a restoring force as it deviates from a horizontal position. It oscillates like a vibrating beam during operation, directly providing the reciprocating movements of the wing with minimal mechanical impedance and replacing the heavy, complex, inefficient transmission systems that electric motor–driven flapping MAVs necessitate to convert the motor's rotary output to oscillatory motion. The wing electrode therefore acts as an elastic energy store, reducing the amount of mechanical work that must be provided through electrostatic actuation. A similar strategy is used by flapping-wing insects such as *Drosophila*, with energy stored in elastic elements within the thorax (*19*).

As a vibrating beam, the wing electrode has a resonant frequency; driving frequencies at or near the resonant frequency allow for higher flapping amplitudes (Fig. 2C); driving frequencies below or above the resonant frequency reduce alignment between electrostatic forcing and the wing electrode's internal oscillatory dynamics, reducing energy exchange and limiting flapping amplitude. However, electrostatic forces are dominant over the resonant dynamics of the wing, and the wing can be controlled to flap at a wide range of frequencies to a high degree of accuracy (Fig. 2D). This behavior is promising for future MAVs that will exhibit controlled flight: Independent modulation of flapping frequency and amplitude (through adjustment of driving frequency and maximum voltage) will allow

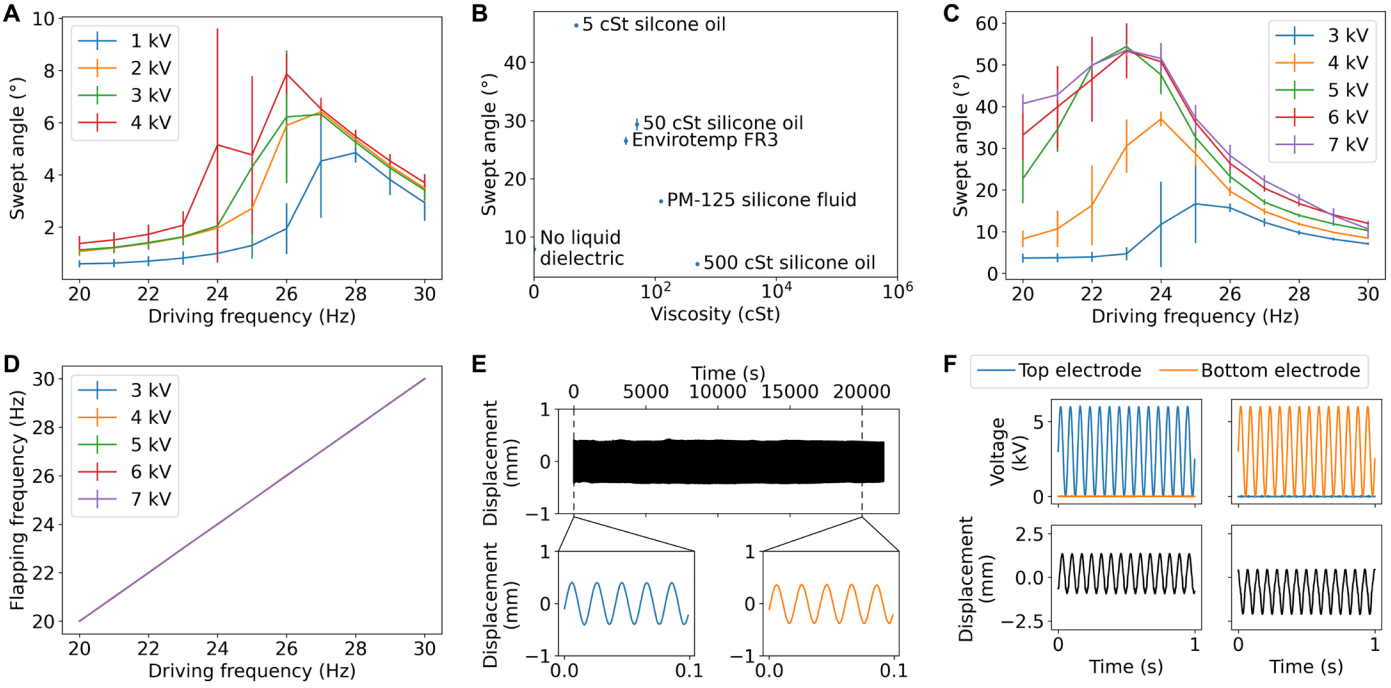

Fig. 2. Characterization of the LAZA. (**A**) Effect of driving frequency upon swept angle for a LAZA system with no liquid dielectric and wing electrode thickness $t = 70$ μm. Maximum voltages up to 4 kV are shown; at maximum voltages of 5 kV and above, electric breakdown became increasingly likely. (**B**) Effect of liquid dielectric viscosity upon swept angle for a LAZA system with $t = 100$ μm, maximum voltage $V_{max} = 6$ kV, and driving frequency $f_d = 33$ Hz. Points are averages of three trials, and error bars show ±1 SD between trials. (**C** and **D**) Effect of driving frequency upon swept angle (C) and flapping frequency (D) for a LAZA system with $t = 70$ μm. In (C) and (D), points are averages from three identical prototypes and error bars show ±1 SD between prototypes. (**E**) Long-term testing, showing no variation in performance over more than 1 million cycles ($t = 150$ μm, $V_{max} = 5$ kV, $f_d = 50$ Hz). Subplots show 100 ms of data before and after 1 million cycles. No liquid dielectric was added during the 6 hours of the long-term test. (**F**) Asymmetric testing, showing how the relative amplitude between upstroke and downstroke can be controlled by favoring the top or bottom electrode, respectively.

for control of flapping MAV position and attitude. This compares favorably with existing electric motor–driven flapping MAVs, which can only alter flapping frequency and cannot alter flapping amplitude without additional control actuators that add further mass to the system (servo motors are typically used).

Because of the high wingbeat frequency of flapping MAVs, it is essential that the LAZA behaves consistently over the thousands of flapping cycles associated with long-term missions. We observed no variation in flapping amplitude over more than 1 million cycles (6 hours of experimental time) at a flapping frequency of 50 Hz (Fig. 2E). This compares favorably with the behavior of DEAs, which have recently been proposed as actuators for flapping MAVs (*13*, *14*): DEAs can exhibit variations in actuation strain and electrical resistance, and even total failure, after thousands of cycles (*20*).

Another unique design aspect of the LAZA in comparison with current flapping MAV actuation systems is the presence of two independent actuators (electrodes) per wing. Increasing the maximum voltage of the top electrode relative to the bottom electrode increases the amount of upstroke relative to downstroke, and vice versa (Fig. 2F). This provides an additional control input for flapping MAV attitude control by adjusting the mean flapping angle, which is a mechanism adopted by insects (*2*).

Wing electrode stiffness

Altering the stiffness of the wing electrode (by altering the beam thickness of the steel strip) has various effects on the behavior of the LAZA. First, the resonant frequency is altered. The experimental resonant frequency (the drive frequency at which flapping amplitude was maximized) showed good agreement with the natural frequency predicted by vibrating beam theory (Fig. 3A), and this was used as the drive frequency when maximum amplitude was required. Stiffer electrodes exhibited lower amplitude flapping because of their increased flexural rigidity, and there was also a reduction in amplitude with less stiff electrodes (Fig. 3B). This was because less stiff wing electrodes had to be driven at lower voltages (Fig. 3C), because higher voltages induced such high forces that the electrodes fully zipped against the top or bottom chassis electrode, and adhesive and cohesive forces associated with the liquid dielectric prevented cyclic motion.

The performance characteristic of interest for flapping MAV actuation systems is specific power (also called power-to-weight ratio), which is the mechanical power applied to the flapping wing by the actuation system, divided by the actuation system mass. High values of specific power imply better performance, as the actuation system mass is reduced, and actuation system mass comprises a large fraction of total system mass. Later in this article, passively pitching wings are added to the LAZA system so that it can exert thrust; however, this makes calculation of specific power more challenging, as work is done on the surrounding air by the wings to produce thrust. Hence, to accurately measure the LAZA's maximum output power, we measured specific power without wings.

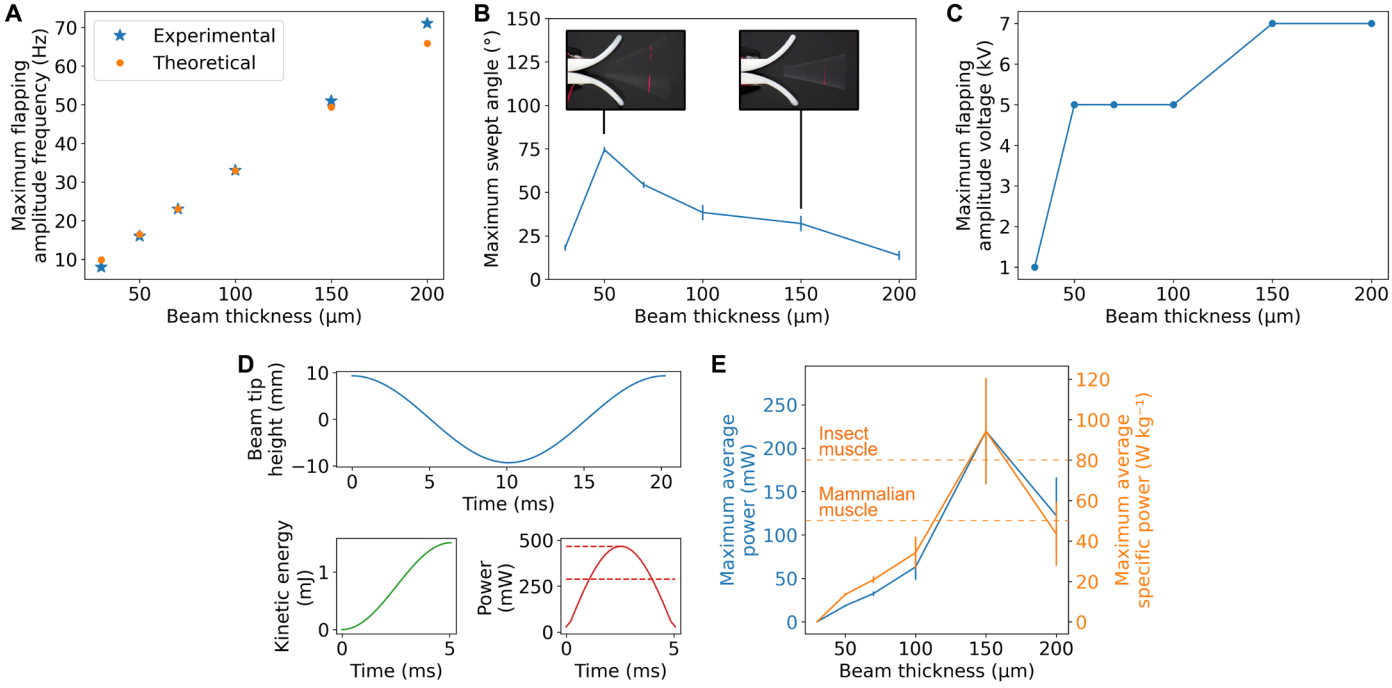

Fig. 3. Effect of wing electrode beam thickness on LAZA performance. (**A**) Experimental and theoretical resonant frequency (the frequency at which flapping amplitude is maximized). (**B**) Maximum (at resonance) swept angle. Insets are photographs of maximum amplitude flapping for wing electrodes of beam thickness $t = 50$ and 150 μm. (**C**) Voltage associated with maximum flapping amplitude. Thicker, stiffer beams can tolerate higher voltages. (**D**) Calculation of peak and average mechanical output power based on beam deflection, for a system with $t = 150$ μm, maximum voltage $V_{max} = 7$ kV, and driving frequency $f_d = 51$ Hz. Peak and average powers of 466.4 and 287.9 mW, respectively, were achieved. (**E**) Maximum (at resonance) average output power and maximum average specific power (maximum average output power normalized by LAZA mass), allowing for comparison with other flapping MAV actuation systems. The highest recorded peak and average specific power were 200.3 and 123.6 W kg^{-1}, respectively, based on a LAZA mass of 2.33 g. Also shown are typical specific power values for flapping insect and mammalian muscle. In (B) and (E), points are averages from three identical prototypes and error bars show ±1 SD between prototypes.

For comparison with biology, mammalian muscle exhibits a typical specific power of 50 W kg^{-1} (*21*), and the specific power of the muscles of flying insects has been estimated between 80 and 83 W kg^{-1} (*22*, *23*). The specific power of artificial flapping MAV actuation systems has been reported as 48.56 W kg^{-1} for electromagnetic actuators for flapping-wing MAVs (*24*), 100 W kg^{-1} for double-cone DEA systems (*13*), 150 W kg^{-1} for piezoelectric actuation (*12*), around 290 W kg^{-1} for electrical motor systems [~1.05-W shaft power given 3.65-g motor mass (*6*)], and 300 to 600 W kg^{-1} for cylindrically rolled DEAs (*14*).

The LAZA output power was calculated using a mathematical model of a vibrating beam (Fig. 3D and Materials and Methods). The highest recorded peak and average power were 466.4 and 287.9 mW, respectively, achieved using a 150-μm-thick wing electrode, actuated at a maximum voltage of 7 kV and driving frequency of 51 Hz. For this system, the LAZA mass (comprising chassis electrodes, insulation, liquid dielectric, and wing electrode) was 2.33 g, implying peak and average specific powers of 200.3 and 123.6 W kg^{-1}, respectively (Fig. 3E). This is considerably higher than the specific power of mammalian and insect flight muscle, and on par with modern flapping MAV actuation systems. In addition to this high specific power, the LAZA provides flapping motion directly and only needs the addition of wings to generate thrust, as opposed to other actuation systems that require a transmission system connecting the actuator to the wings.

Demonstration of thrust generation

The LAZA produces transmission-free reciprocating motion of the wing electrode; however, the LAZA alone produces negligible thrust, because the aerodynamic forces associated with movement of the wing electrode are mostly equal and opposite during upstroke and downstroke. In insect flight, wing pitching is necessary to rectify net directional thrust during flapping (Fig. 4A). Similarly, LAZA-driven MAVs must also include pitching wings (Fig. 4B).

Passive wing pitching was achieved by attaching the wing to a carbon fiber rod, which was free to rotate within an aluminum tube (Fig. 4C). To minimize the mass of the wing, it was made from thin biaxially oriented polyethylene terephthalate (BoPET), strengthened by three nickel silver spars that attached to the carbon fiber rod. The aluminum tube was complete at its ends but had material removed along its length to minimize mass (sections B-B and C-C). The aluminum tube was attached to a three-dimensional (3D)–printed wing adapter, which featured symmetrical protrusions that limited the pitching angle (section B-B). The 3D-printed wing adapter was then attached to the wing electrode, which provided the wing's flapping movement. Figure 4D shows an exploded and assembled computer-aided design (CAD) drawing of the passively pitching wing design. To accommodate the addition of passively pitching wings, the length of the wing electrode $l_{electrode}$ was reduced from 50 to 15 mm. The shorter electrode compensated for the added mass and allowed for higher flapping frequencies compared with

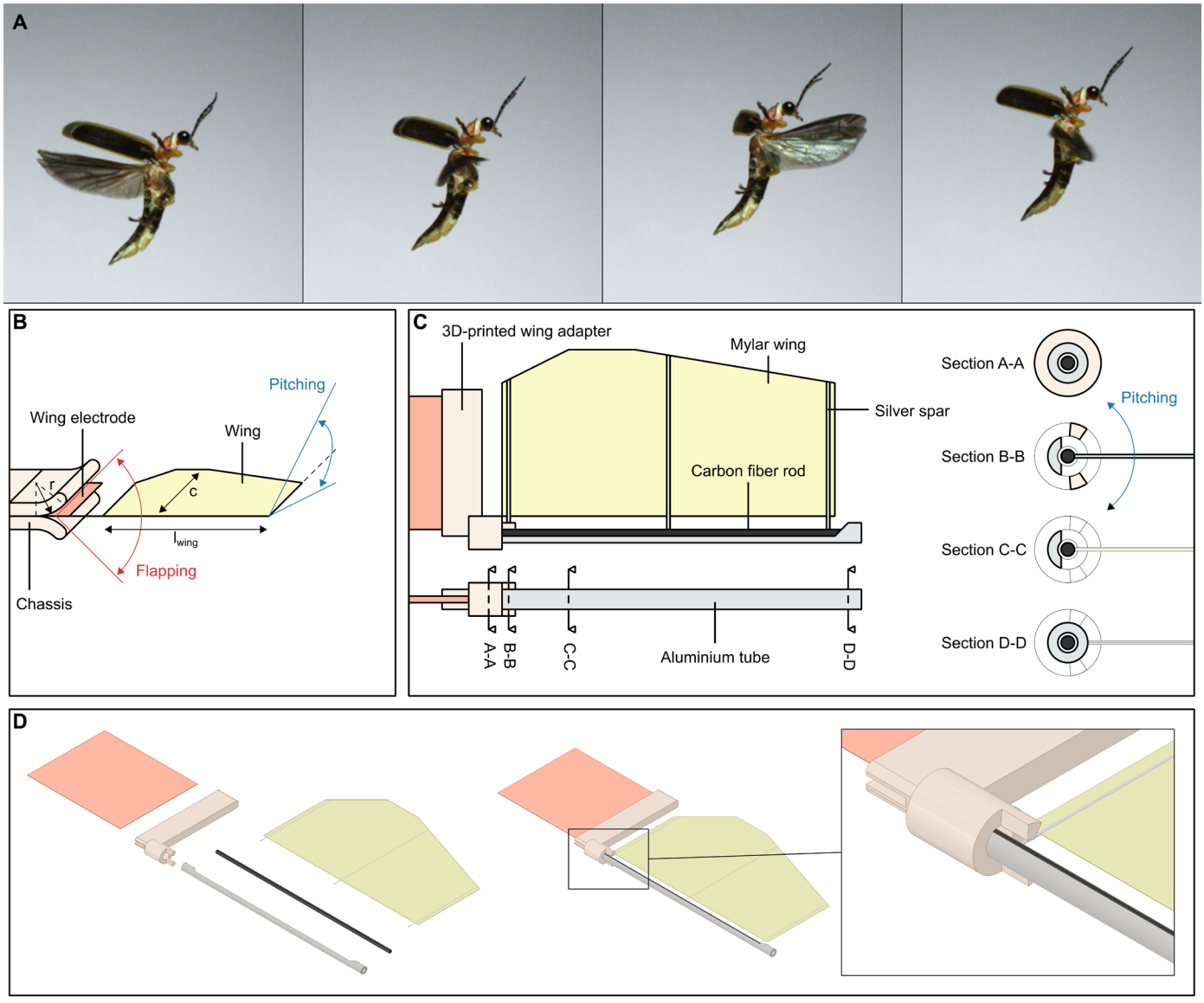

Fig. 4. Passively pitching wings for LAZA thrust generation. (**A**) Images from slow-motion video of *Photinus pyralis* in vertical flight, showing wing pitching during flapping (image credit: Adrian Smith, North Carolina Museum of Natural Sciences). (**B**) Overview of flapping and pitching in LAZA system. Wing length, l_{wing}, wing chord length, *c*, and chassis electrode radius of curvature, *r*, are shown. (**C**) General design of the passively pitching wings presented in this work. Section cuts (A-A to D-D) are indicated along the length of the wing and shown on the right. (**D**) Exploded and assembled computer-aided design (CAD) drawing of the passively pitching wing design, with close-up of the symmetrical 3D-printed wing adapter protrusions.

the behavior when passively pitching wings were added to 50-mm wing electrodes.

The dimensions of the wing, wing electrode, and chassis were varied to maximize the thrust provided by LAZA flapping (Fig. 4B). Increasing the wing length, l_{wing}, and wing chord length, *c*, increases the wing surface area and therefore can increase thrust. However, this also increases the wing's inertia, making the wing harder to flap and reducing its resonant frequency. Increasing the radius of curvature of the chassis electrodes, *r*, reduces the spacing between the wing electrode and chassis electrodes, increasing electrostatic force (according to Coulomb's inverse-square law). However, this also limits the maximum flapping angle of the wing. Increasing the maximum swept pitching angle of the wing, ψ, also influences the amount of thrust generated. The maximum thrust generated for a subset of tested passively pitching LAZA systems is shown in fig. S1A. The highest achieved thrust was 5.73 mN (l_{wing} = 50 mm, *c* = 20 mm, *r* = 10 mm, *t* = 50 μm, ψ = 110°, V_{max} = 8 kV, f_d = 13 Hz). Flapping amplitude was also maximized at this driving frequency. Altering the chassis electrode curvature in either direction (*r* = 8 mm or *r* = 12 mm) reduced thrust. The resultant LAZA system had a wingspan of around 150 mm, similar in size to a large dragonfly. Figure 5A and Movie 4 show a front view of the LAZA system that achieved maximum thrust. The swept angle of the wings was around 80°.

During flapping, the wings passively pitched because of aerodynamic drag. The maximum pitching angle was limited to ±55° by the protrusions of the 3D-printed wing adapter (ψ = 110°), and a

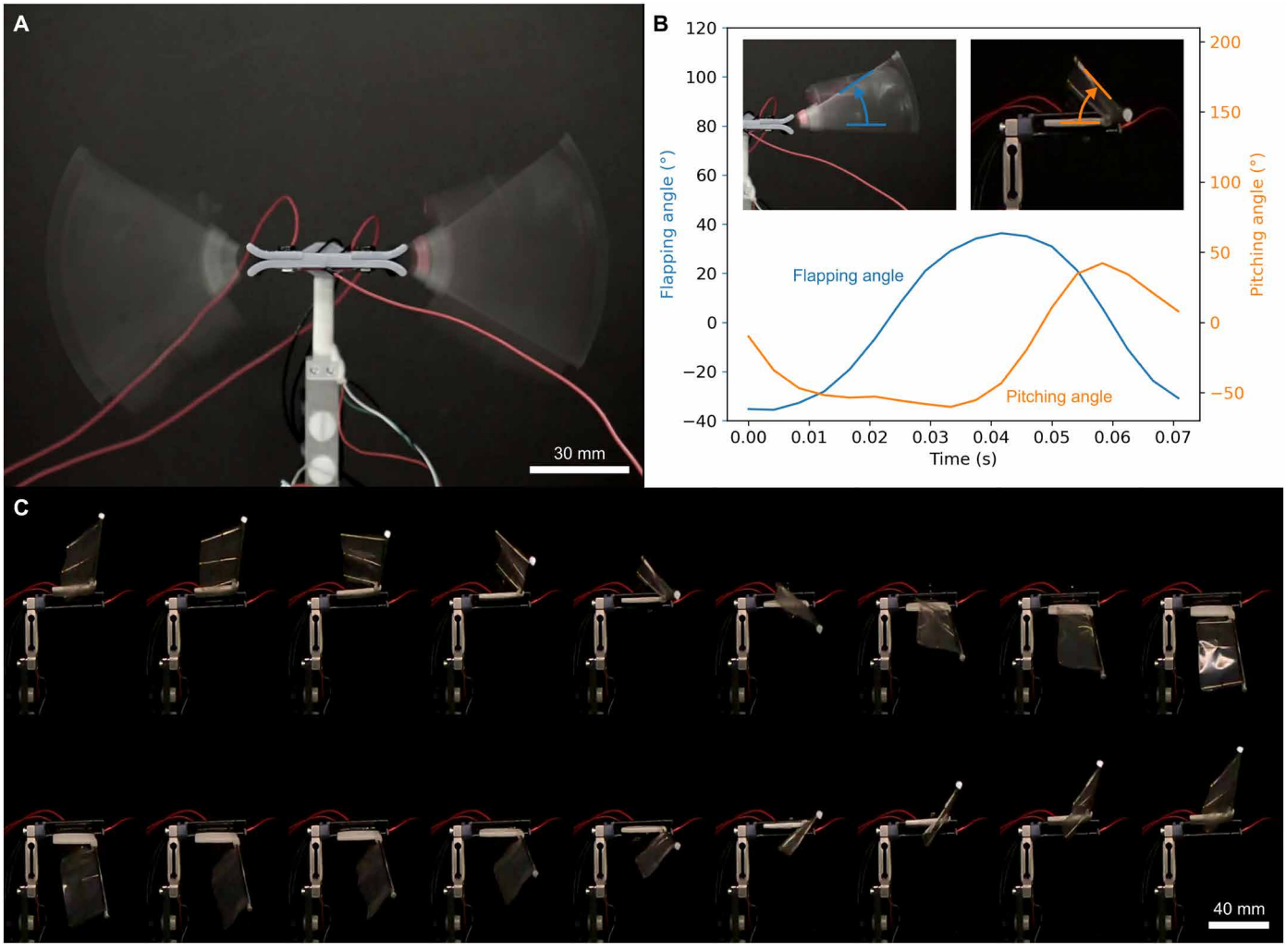

Fig. 5. LAZA thrust generation. (**A**) A composite front view image of the LAZA system that achieved maximum thrust (l_{wing} = 50 mm, c = 20 mm, r = 10 mm, t = 50 μm, ψ = 110°, V_{max} = 8 kV, f = 13 Hz), comprising the average of 1 s of video filmed at 50 FPS. The swept angle of the wings is around 80°. (**B**) Estimated flapping angle and pitching angle during a single flapping period. Insets are images showing how flapping angle and pitching angle are defined. The asymmetry in maximum pitching angle (+42° versus −60°) is attributed to gravity acting on the passively pitching wing. (**C**) Side view frames from video filmed at 240 FPS over one flapping period.

pitching angle close to this was achieved through most of the upstroke (Fig. 5B). During downstroke, a pitching angle close to 50° was achieved, and the amount of time for which this pitching angle was maintained was lower than during upstroke. This asymmetry is attributed to the weight of the pitching wing, which assists pitching during upstroke and impedes it during downstroke. Figure 5C shows frames from footage recorded at 240 frames per second (FPS) over one flapping period. A video is provided as Movie 5.

For comparison with other flapping MAV actuation systems, the thrust-to-power ratio of this LAZA system was calculated (Materials and Methods). The average electrical power delivered to the LAZA during this trial was 242.9 mW, resulting in a thrust-to-power ratio of 23.59 N kW^{-1} (2.41 g W^{-1}). This thrust-to-power ratio was achieved at an effective disk loading of 0.73 N m^{-2}. A plot comparing thrust-to-power ratio with effective disk loading is included as fig. S1B. This value approaches the thrust-to-power ratio achieved by traditional direct-drive propellor systems such as helicopter rotors (7.3 g W^{-1}) (*25*) and quadrotor MAVs (10–20 g W^{-1}) (*26*). Comparing with artificial flapping MAV actuation systems, the thrust-to-power ratio for a recent electric motor–driven flapping-wing MAV has been reported as 3.48 g W^{-1} (34.14 N kW^{-1}) (*9*), the Harvard RoboBee has achieved 4.2 g W^{-1} (41.20 N kW^{-1}) (*27*, *28*), and a previous micro-scale parallel-plate electrostatic flapping-wing actuator delivered 79.2 μN while consuming an estimated 1.52 mW of electrical power, implying a thrust-to-power ratio of 52.1 N kW^{-1} (*29*). Another performance metric for comparison is the thrust-to-weight ratio. In this device, the mass of each LAZA was 1.37 g, and the total wing mass was 2.37 g, implying a thrust-to-weight ratio of 0.114 (Materials and Methods), similar to that of the micro-scale parallel-plate electrostatic flapping-wing actuator, which achieved a thrust-to-weight ratio of 0.161 (79.2 μN, 50 mg) (*29*). Table 1 lists key performance metrics for the LAZA.

Last, to evaluate the potential for LAZA-generated thrust to deliver flight, a horizontally moving LAZA system was constructed (Fig. 6A). Electrical power was provided by lightweight enameled copper wires, and the weight of the LAZA system was supported by

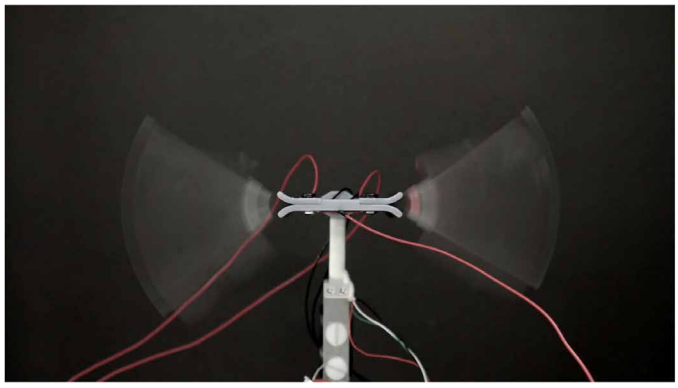

Movie 4. Passively pitching LAZA flapping system, front view. Front view of a passively pitching LAZA system with chassis electrode radius of curvature 10 mm, wing electrode thickness 50 μm, maximum swept pitching angle 110°, maximum voltage 8 kV, and flapping frequency 13 Hz. The system generates an average thrust of 5.73 mN.

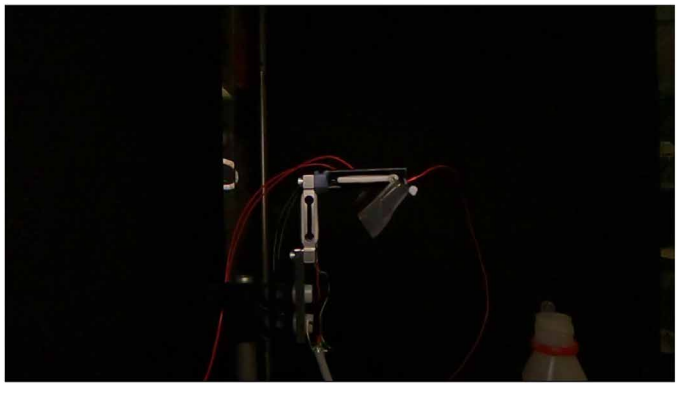

Movie 5. Passively pitching LAZA flapping system, side view, slow motion. Side view of a passively pitching LAZA system with chassis electrode radius of curvature 10 mm, wing electrode thickness 50 μm, maximum swept pitching angle 110°, maximum voltage 8 kV, and flapping frequency 13 Hz. The system generates an average thrust of 5.73 mN. Recorded at 240 FPS and played at 30 FPS (1/8× speed slow motion).

Table 1. Key performance metrics for the LAZA.

Performance metric	Value
Maximum average specific power	123.6 W kg^{-1}
Thrust-to-power ratio	23.59 N kW^{-1} (2.41 g W^{-1})
Thrust-to-weight ratio	0.114

a taut horizontal nylon guidewire. The system was free to move in the horizontal direction. Figure 6 (B and C) shows images from slow-motion footage of the LAZA system accelerating from at-rest (Movie 6A) and moving horizontally after accelerating over a distance of around 2 m (Movie 6B). The maximum speed of the LAZA system was 0.71 m/s (around 18 body lengths per second). Figure S6C and Movie 6C show the path of the LAZA system's wing tip as it moves horizontally.

Scaling analysis

The presented results demonstrate the function and describe the effect of varying system parameters for a dragonfly-sized flapping MAV. To provide insight and guide future work, a scaling analysis of LAZA-driven flapping MAVs is presented. Considering the dimensional quantities of Eq. 1 and a MAV with characteristic length L, area A scales with L^2, and $t_{insulator}$ and t_{medium} scale with L. The maximum voltage that may be applied is based on the breakdown strength of the medium and scales with L. Applying dimensional analysis to Eq. 1 leads to

$$F \propto \frac{L^2 L^2}{(L+L)^2} \tag{2}$$

This implies that electrostatic force scales according to $F \propto L^2$. Notably, V contributes to F scaling with respect to L^2, whereas $t_{insulator}$ and t_{medium} contribute to F scaling with respect to $\frac{1}{L^2}$; therefore, their effects counteract one another, and the relevant scaling effect is that of F with respect to area A (L^2).

In practice, LAZAs feature a progressive zipping region such that increasing the width of the wing electrode increases zipping area, whereas increasing the length of the wing electrode has no effect on zipping area. The result of this practical limitation implies that electrostatic force scales with L rather than L^2.

System weight, which directly affects the amount of thrust required for self-supporting flight, scales with L^3. This implies that the ratio of electrostatic force to system weight scales as follows

$$\frac{F}{mg} \propto \frac{L}{L^3}$$

$$\therefore \frac{F}{mg} \propto L^{-2} \tag{3}$$

where m is the mass and g is the gravitational acceleration. The current 150-mm wingspan LAZA flapping system achieved a thrust-to-weight ratio of 0.114. The above analysis suggests that thrust-to-weight ratios approaching 1 could be achieved by reducing the system scale by around one-third, resulting in a 50-mm wingspan device capable of self-supporting flight.

DISCUSSION

This article describes an actuation system for flapping MAVs called the LAZA. The LAZA leverages liquid-amplified electrostatic actuation to directly apply time-varying forces on a central wing electrode that forms part of the wing root, resulting in continuous reciprocating wing motion. Thrust generation can be achieved by the addition of a passively pitching wings.

The LAZA has several advantages compared with previous flapping MAV actuation systems (comprising actuator and transmission). Compared with conventional motor-transmission systems, the LAZA is lightweight and efficient, completely lacking any transmission system and their associated added mass and energetic inefficiency. Compared with more recently demonstrated DEA systems, the LAZA provides high reliability, exhibiting no change in performance over more than 1 million actuation cycles. In contrast, DEAs can exhibit variations in actuation strain and electrical resistance, and even total failure, after thousands of cycles (*20*).

The LAZA requires a tiny droplet of liquid dielectric to amplify electrostatic force, and if removed, the performance of the device

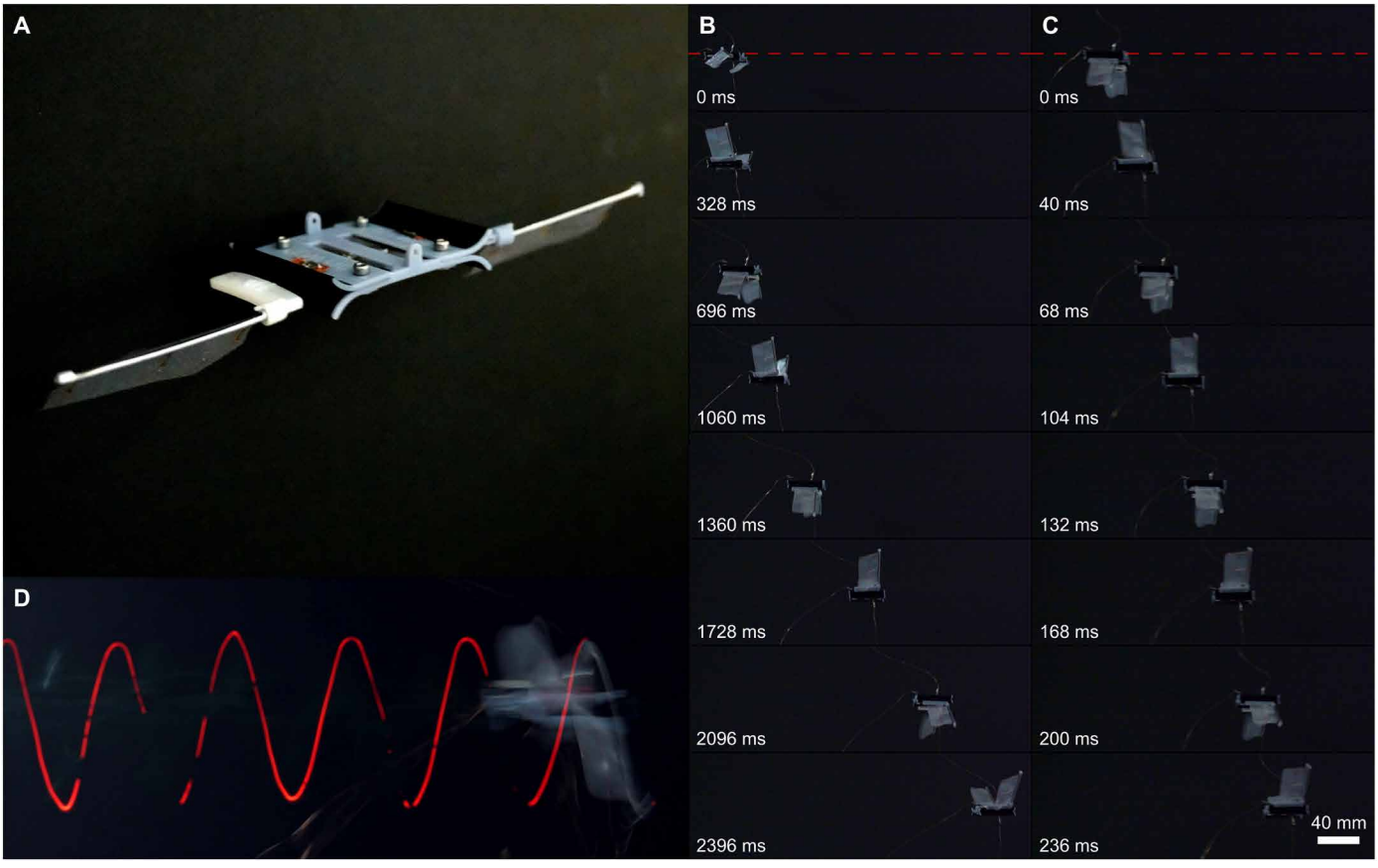

Fig. 6. Horizontally moving LAZA system. (**A**) Photograph of horizontally moving LAZA system. (**B**) Images from slow-motion footage of the LAZA system accelerating from at rest. (**C**) Images from slow-motion footage of the LAZA system after accelerating over a distance of around 2 m, reaching a speed of 0.71 m/s (18 body lengths per second). (B) and (C) were filmed at 250 FPS, and time beyond the first images is indicated in the bottom left. The dashed red line indicates the location of the nylon guidewire. (**D**) Composite image showing the path the LAZA system's wing tip as it moves horizontally. Component images are provided as fig. S2. Video footage related to (B) to (D) is provided as Movie 6.

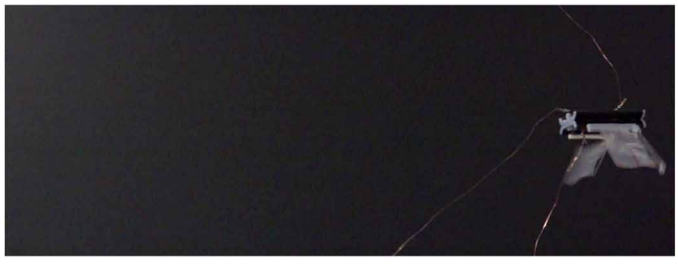

Movie 6. Horizontally moving LAZA system. (**A**) Horizontally moving LAZA system accelerating from rest, 1× speed. (**B**) LAZA system moving horizontally after accelerating over a distance of 2 m, recorded at 250 FPS. Played three times at 1× speed and then once at 1/10× speed. (**C**) LAZA system moving horizontally with a red light-emitting diode (LED) mounted on its wing tip. Played three times at 1× speed. A long-exposure (1 s) photograph showing the LED path is subsequently shown.

will be impaired. Although a sudden impact might forcibly remove the liquid dielectric, it has been shown here that performance is not altered over more than 1 million actuation cycles, implying that long-term missions should be feasible for LAZA-driven flapping MAVs. The LAZA exhibits peak and average specific power (a key performance metric for flapping MAV actuation systems) of 200.3 and 123.6 W kg^{-1}, respectively, considerably higher than that of biological systems and on par with modern flapping MAV actuation systems.

We created a LAZA flapping system that converted actuation to directional thrust by adding passively pitching wings to the LAZA. Various wing designs were evaluated, and a maximum thrust of 5.73 mN was achieved. The electrical power delivered to the LAZA to achieve this thrust was 242.9 mW, implying a thrust-to-power ratio of 23.59 N kW^{-1}, approaching that of helicopter rotors and quadrotor MAVs and similar to that of recent state-of-the-art flapping MAVs, which feature transmission systems with their associated disadvantages.

A horizontally moving LAZA flapping system was tested, which demonstrated acceleration from at-rest and horizontal movement at speeds up to 0.71 m/s (around 18 body lengths per second). Here, the weight of the system was supported by a nylon guidewire, analogous to the surface tension that supports the weight of surface skimming insects, which have been proposed as an intermediate stage in insect flight evolution (*30*). The horizontally moving LAZA system may be considered at a similar stage; future LAZA systems could integrate airfoils to provide lift and support the weight of the system when traveling at speed. For future systems with onboard power electronics, custom high-voltage amplifiers will be required to minimize mass; subgram drive electronics have been demonstrated for terrestrial robots driven by high-voltage electrostatic actuators (*31*).

Further to those evaluated here, the LAZA exhibits several additional advantages compared with existing flapping MAV actuation systems. Liquid-amplified electrostatic zipping systems can be made using a wide range of materials: conducting and insulating tapes, 3D-printed polylactic acid, and even pencil and office paper (*15*). In addition to a considerable reduction in cost compared with, for example, high-performance motors, this also allows for wide flexibility in materials for future design innovation. The LAZA is also extremely simple to manufacture and repair; the presented design requires only the application by hand of adhesive tapes to the flapping MAV chassis. Furthermore, the LAZA itself is inherently silent; therefore, ultraquiet flapping MAVs are possible through noise-reducing wing design, as is exhibited by owls to promote silent flight (*32*). This would enable, for example, voice tracking in search-and-rescue missions. Last, the flexible actuator and lack of a fragile transmission system reduce the potential for midflight collisions to damage the flapping MAV, as has been demonstrated in MAVs driven by soft actuators (*14*). The transmission-free flapping MAV concept and the advantages of the LAZA over currently existing flapping MAV actuation systems provide a platform for the next generation of high-performance flapping MAVs. The elimination of transmission-associated mass and transmission-associated losses will lead to faster, more maneuverable MAVs capable of longer duration exploration and inspection tasks, such as autonomous monitoring of wind turbines.

Another advantage of the LAZA concept that has been demonstrated here is the ability to independently control flapping frequency, flapping amplitude, and the relative amplitude of upstroke compared with downstroke. This will enable precise attitude and position control (*28*, *33*), which will be the subject of future investigations. The pitch of the flapping MAV will be controlled by altering the relative amplitude of upstroke and downstroke (fig. S3A), whereas roll will be controlled by altering the relative amplitude of opposing wings (fig. S3B). Yaw control requires modulation of the velocity of upstroke compared with downstroke, which has not been demonstrated here, and will also be the topic of further study (fig. S3C). Nonetheless, control of pitch, roll, and thrust is already sufficient for precise three-axis position control such that a LAZA-driven flapping MAV may be controlled to reach any location within an environment.

A remaining challenge for a LAZA-driven flapping MAV is the demonstration of self-supporting liftoff and flight. The LAZA thrust-to-weight ratio demonstrated here was 0.114, whereas values exceeding 1 are required for vertical takeoff. Nonetheless, the current LAZA-based flapping MAV was capable of horizontal acceleration and could use the thrust provided to reduce fall speed and make gliding flight more sustained. In its present embodiment, the LAZA can also be readily exploited in a wide variety of land- and water-based robotics applications, including artificial water skaters. Increased performance and reduced mass are both required to improve thrust to weight and allow for self-supporting flight. Scaling analysis suggests that reducing the scale of a future LAZA-based flapping MAV could increase the thrust-to-weight ratio, with a 50-mm wingspan device (compared with the current 150 mm) being capable of self-supporting flight.

In the future, the performance of the LAZA will be improved by further design investigation, such as varying the materials forming the electrodes, insulation, and liquid dielectric. Chassis electrodes of negligible mass are easily achievable as nanometer-thick metalized coatings (*34*). Improving the dielectric properties of the insulation will directly enhance electrostatic force (*15*) and additionally allow for thinner, lower-mass insulators, such as ultrathin dielectric coatings. Improving the dielectric properties of the liquid dielectric will allow the application of higher voltages, strengthening electric field and further improving electrostatic force, and ultralow viscosity fluids will ensure maximum output mechanical power. These improvements will reduce LAZA mass and also allow for similar mechanical performance at lower applied voltages, required for the minimization and mass reduction of power electronics, which is essential if they are to be moved onboard. In addition, reduction of the voltages required for operation will reduce safety considerations associated with high voltage, allowing these devices to be used in closer proximity to humans. That being said, the high-voltage amplifiers used in this work had a maximum current limitation of 100 μA, considerably lower than the maximum continuous current of 20 mA specified by the Underwriters Laboratories and International Electrotechnical Commission safety standards (*35*).

Our proof-of-principle LAZA system has a 3D-printed polymer body, which will in the future be optimized for its mass-specific strength and stiffness. Material databases such as Ashby selection charts give us confidence that the mass of the LAZA can be reduced by over one order of magnitude. Furthermore, the prototype wings demonstrated here also have great potential for improvement in terms of mass-specific thrust. Wing design was not the focus of this work, and thus, there is the potential for considerable increases in thrust and aerodynamic efficiency though co-optimization of the chassis and wing (*27*)—for example, "clap and fling" strategies that have been shown to improve performance in flapping MAVs (*2*, *36*, *37*). The mass of the passively pitching wings can be reduced using stronger, more lightweight materials, or alternative wing designs such as flexure-based systems (*12*). In addition, increased functionality could be pursued; the simplicity of the passively pitching wings could enable inverting wing cambers or beetle-inspired wing folding for improved robot transportability. Another area for investigation is parallelization: LAZA-driven flapping MAVs could feature multiple LAZAs in parallel, coupled to a wing through a rod or tension cord. This would increase the force applied to the wing and potentially enable higher values of thrust. Last, the flapping MAV energy supply and control electronics will be moved onboard, allowing for a fully untethered device, as has recently been achieved through the use of photovoltaic cells in the Harvard RoboBee (*33*). This will enable a class of low-cost, lightweight, high-performance transmission-free flapping MAVs for long-term remote exploration and search-and-rescue missions.

MATERIALS AND METHODS

Manufacture of LAZA systems

Structural components were 3D-printed using a commercial LCD resin 3D printer (ANYCUBIC Photon, ANYCUBIC, China) and an ultraviolet (UV)–curing resin (ELEGOO LCD UV 405 nm Rapid 3D Resin, White, ELEGOO, China) and assembled using stainless steel nuts and bolts. Chassis electrodes comprised a single layer of conductive copper foil tape (HB 720A, Hi-Bond Tapes, UK) and were insulated using a single layer of polyvinyl chloride (PVC) tape (AT7, Advance Tapes, UK). The wing electrode was a 70-mm-long, 25-mm-wide C100S carbon steel strip (C-steel 1.1274, h+s Präzisions-Folien GmbH, Germany). Ten millimeters of the carbon steel strip protruded from the back of the LAZA system, and 10 mm was clamped between the top and bottom chassis electrode; therefore,

the functional wing electrode length $l_{electrode}$ was 50 mm. Various thicknesses of wing electrodes were used. Before each set of experiments, a small quantity (around 0.4 ml) of 5 cSt silicone oil (317667, Sigma-Aldrich, USA) was added by pipette, where the wing electrode and chassis electrodes meet.

LAZA characterization

The LAZA was characterized using a custom-built high-voltage testing setup at Bristol Robotics Laboratory. The setup comprised a laboratory computer running MATLAB, which interfaced with a multifunction I/O device (NI USB-6343, National Instruments, USA). This device recorded voltage from sensors and controlled high-voltage amplifiers (10HVA24-BP1, UltraVolt, USA), which supplied high voltage to the LAZA electrodes. The wing electrode was connected to ground, whereas voltages were applied to the top and bottom chassis electrodes. The movement of the wing electrode was recorded using a laser displacement meter (LK-G402, Keyence, Japan). The laser beam was pointed directly downward and was targeted 10 mm from the end of the wing electrode such that displacement could be reliably recorded even during flapping (the wing electrode tip moves both vertically and horizontally as the wing electrode flexes, making measurement of wing electrode tip position challenging). In later experiments, thrust was recorded using a load cell (TAL221, HT Sensor Technology Co. Ltd., China) and load cell amplifier (RW-ST01A, Brightwin Electronics, China). A diagram of the experimental setup for LAZA characterization is provided in the Supplementary Materials (fig. S4).

To ensure repeatability, 0.4 ml of silicone oil was added by pipette to the LAZA before each set of experiments. A set of experiments typically comprised flapping at multiple frequencies: 7 s of flapping at each frequency, with 3 s of downtime between frequencies. For example, for the experiment with the LAZA-driven flapping MAV that achieved maximum thrust, 11 frequencies from 10 to 20 Hz were tested for 7 s each, implying 0.4 ml of silicone oil for more than 1000 actuation cycles. During long-term testing, 0.4 ml of silicone oil was added before the experiment, and there was no variation in performance over more than 1 million actuation cycles.

A maximum actuation voltage of 7 kV was applied; above this voltage, the likelihood of electric breakdown increased. In experiments where no liquid dielectric was present, this maximum actuation voltage was further reduced to 4 kV.

Modeling movement and power of the wing electrode

A mathematical model was used to model the movement, energy, and power of the wing electrode when at resonance. A full derivation is provided in the Supplementary Materials. In the model, the position of the wing electrode is described by the following equation

$$w(x,t) = \frac{1}{2}B_1\cos(\omega_1 t)\left(\cosh\beta_1 x - \cos\beta_1 x - C_{\text{mode}}(\sinh\beta_1 x - \sin\beta_1 x)\right) \quad (4)$$

where $w(x, t)$ is the position of the wing electrode and varies with displacement along the electrode x and time t. B_1 is the flapping amplitude at the wing electrode tip, ω_1 is the first resonant frequency of the wing electrode, and β_1 and C_{mode} are constants. β_1 is defined by

$$\beta_1{}^4 = \frac{\rho A \omega_1{}^2}{EI} \quad (5)$$

where ρ is the density of the wing electrode, A is its cross-sectional area, E is its Young's modulus, and I is its second moment of area for the direction of bending. C_{mode} is defined by

$$C_{\text{mode}} = \frac{\cosh(\beta_1 L) + \cos(\beta_1 L)}{\sinh(\beta_1 L) + \sin(\beta_1 L)} \quad (6)$$

where L is the free length of the wing electrode. To calculate flapping angle, the wing slope $\frac{\partial w}{\partial x}$ was first calculated

$$\frac{\partial w}{\partial x}(x,t) = \frac{1}{2}\beta_1 B_1\cos(\omega_1 t)\left(\sinh\beta_1 x + \sin\beta_1 x - C_{\text{mode}}(\cosh\beta_1 x - \cos\beta_1 x)\right) \quad (7)$$

Flapping angle, $\theta(t)$, the angle of the wing electrode at its tip ($x = L$), was then calculated using

$$\theta(t) = \tan^{-1}\frac{\partial w}{\partial x}(L,t) \quad (8)$$

The swept angle reported in Figs. 2C and 3B is twice the maximum value of flapping angle. The kinetic energy in the wing electrode, E_k, was calculated using

$$E_k = \frac{1}{2}\rho A\int_0^L\left(\frac{\partial w}{\partial t}\right)^2 dx \quad (9)$$

where

$$\frac{\partial w}{\partial t}(x,t) = -\frac{1}{2}B_1\omega_1\sin(\omega_1 t)\left(\cosh\beta_1 x - \cos\beta_1 x - C_{\text{mode}}(\sinh\beta_1 x - \sin\beta_1 x)\right) \quad (10)$$

This integration was performed numerically in Python, dividing the wing electrode into 51 separate sections and a single time period into 101 separate time steps. At each time step, kinetic energy was calculated using the Python NumPy numpy.trapz function. Subsequently, power was also calculated numerically, taking the gradient of kinetic energy using the Python NumPy numpy.gradient function. The results of these calculations for a LAZA system with t = 150 μm, maximum voltage V_{max} = 7 kV, and driving frequency f_d = 51 Hz are shown in Fig. 3D.

Calculating specific power

Specific power is defined as the power of the LAZA divided by the LAZA mass. The LAZA comprised two insulated chassis electrodes, a tiny droplet of liquid dielectric, and one wing electrode. Each chassis electrode was a single layer of conductive copper foil tape (HB 720A, Hi-Bond Tapes, UK), insulated with a single layer of PVC tape (AT7, Advance Tapes, UK). The masses of the two chassis electrodes and two sections of insulating tape were determined in the laboratory using a precision balance (HCB 123, Adam Equipment, UK) and were recorded as 0.22 g for the chassis electrodes and 0.3 g for sections of insulating tape. The liquid dielectric was around 0.4 ml of 5 cSt silicone oil (317667, Sigma-Aldrich, USA), density 0.913 g ml^{-1}, implying a liquid dielectric mass of 0.37 g. The wing electrode was a 50-mm-long, 25-mm-wide C100S carbon steel strip (C-steel 1.1274, h+s Präzisions-Folien GmbH, Germany). Its mass depended on its thickness; for the highest power system, a 150-μm-thick wing electrode was used, implying a wing electrode volume of 187.5 mm^3. The density of C100S carbon steel is 7700 kg m^{-3}, implying a wing electrode mass of 1.44 g. This results in an overall

LAZA mass of 2.33 g, converting peak and average powers of 466.4 and 287.9 mW to peak and average specific powers of 200.3 and 123.6 W kg^{-1}, respectively.

Passively pitching wing manufacture

The passively pitching wing was made from 23-μm-thick BoPET (785-0782, RS PRO, UK), strengthened by three 0.2-mm-diameter nickel silver spars (75850, Antics Online, UK). The nickel silver spars were "sewn" into the BoPET by inserting them through small incisions, with these insertion points being reinforced with cyanoacrylate glue (Loctite 406, Loctite, Germany). The nickel silver spars were glued into 0.2-mm holes drilled into a 1-mm-diameter carbon fiber rod (45871, Antics Online, UK). The carbon fiber rod was inserted into a 2-mm-diameter, 0.45-mm-wall-thickness aluminum tube (75544, Antics Online, UK), which was complete at the ends but had material removed along its length, allowing the carbon fiber rod to rotate freely while minimizing the mass of the aluminum rod. The aluminum rod was glued into a hole forming part of a 3D-printed wing adapter, which attached to the wing electrode. The 3D-printed wing adapter featured protrusions that constrained the maximum pitching angle. To accommodate the addition of passively pitching wings, the length of the carbon steel strip used for the wing electrode was reduced from 70 to 30 mm. Five millimeters of the carbon steel strip protruded from the back of the LAZA system, and 10 mm was clamped between the top and bottom chassis electrode; therefore, the functional wing electrode length $l_{electrode}$ was 15 mm.

Measurement of thrust generated by passively pitching wings

Passively pitching wings were attached to the wing electrodes of a symmetrical system featuring two LAZAs. The thrust of the system was recorded using a load cell (TAL221, HT Sensor Technology Co. Ltd., China) and load cell amplifier (RW-ST01A, Brightwin Electronics China). The force measured by the load cell included oscillatory forces induced by the upward and downward motion of the wings. To calculate the thrust generated by the system, a moving average of force data was calculated over a 1-s window (considerably higher than the flapping period). The average force in the final second of testing was compared with the average force over a second during which the system was inactive: The difference between these two values was recorded as thrust. During these experiments, we were able to increase maximum voltage to 8 kV without breakdown to demonstrate the maximum thrust potential of the LAZA.

Estimation of flapping angle and pitching angle from video footage of LAZA experiments

Machine vision was used to estimate flapping angle and pitching angle from video footage of LAZA experiments. Individual frames were exported from slow-motion video of the LAZA, filmed from the side. Blue markers were manually added to each frame showing the location of the wing leading and trailing edge. A Python function was then used to estimate marker location using the OpenCV SimpleBlobDetector class, and marker locations were used to infer flapping angle and pitching angle through trigonometry, based on the geometry of the flapping system.

Calculation of LAZA thrust-to-power ratio

The electrical power delivered to the LAZA was calculated by taking the product of applied voltage and flowing current for each electrode, which was recorded using the high-voltage amplifiers (10HVA24-BP1, UltraVolt, USA). The powers delivered to each electrode were summed to give the total electrical power delivered, which was 242.9 mW for the trial that produced the best thrust. The thrust produced was 5.73 mN, implying a thrust-to-power ratio of 23.59 N kW^{-1}.

Calculation of LAZA disk loading

As is common for bird and insect wings in momentum theory, effective disk area is calculated using wing length as disk radius (*38*). Given the wing length of 50 mm, this implies an effective disk area of 78.54 cm^2. Thrust was used rather than weight to calculate disk loading because LAZA systems are not yet capable of hovering flight.

Calculation of LAZA thrust-to-weight ratio

Apart from the wing electrode, the LAZA masses in the specific power calculation section remain unchanged (chassis electrodes: 0.22 g, insulating tape: 0.3 g, liquid dielectric: 0.37 g). The wing electrode used for the passively pitching LAZA system was 50 μm thick, three times thinner, implying a wing electrode mass of 0.48 g, and a total LAZA mass of 1.37 g. The passively pitching LAZA system featured two LAZAs (2.74 g) and passively pitching wings weighing 2.37 g, implying a total mass of 5.11 g. Given the thrust produced of 5.73 mN, this results in a thrust-to-weight ratio of 0.114.

Horizontally moving LAZA system

A horizontally moving LAZA system was constructed to evaluate the capability of LAZA-generated thrust to deliver flight. Electrical power was provided to the LAZA system through lightweight enameled copper wire (CUL100/0.10, Block, UK). The weight of the LAZA system was supported by taut black nylon thread (HSTHRE0023, Supercrafts, UK), which ran through eyelets on the 3D-printed LAZA chassis. The nylon guidewire was suspended horizontally across the laboratory, with a slight incline to minimize frictional forces, such that the LAZA could move with negligible resistance in the direction of travel (sufficient friction remained to bring the system to a halt in the absence of thrust). The motion of the LAZA system was recorded using a high-speed camera (RX10 IV, Sony Corporation, Japan).

Estimating maximum speed of horizontally moving LAZA system

Movie 6B was used to estimate the maximum speed of the LAZA system. On the basis of the LAZA system's length (40 mm), the distance traveled by the LAZA system was estimated to be around 327 mm. The number of frames between the LAZA system's frontmost point entering the frame and leaving the frame was 115 frames. The video was recorded at 250 FPS; therefore, the time taken was 0.46 s, implying a speed of 0.71 m/s or 17.8 body lengths per second.

SUPPLEMENTARY MATERIALS

www.science.org/doi/10.1126/scirobotics.abi8189
Materials and Methods
Figs. S1 to S5

REFERENCES AND NOTES

1. M. H. Raibert, Legged robots. *Commun. ACM* **29**, 499–514 (1986).
2. C. P. Ellington, The novel aerodynamics of insect flight: Applications to micro-air vehicles. *J. Exp. Biol.* **202**, 3439–3448 (1999).

3. D. Floreano, R. J. Wood, Science, technology and the future of small autonomous drones. *Nature* **521**, 460–466 (2015).
4. J. T. Vance, I. Faruque, J. S. Humbert, Kinematic strategies for mitigating gust perturbations in insects. *Bioinspir. Biomim.* **8**, 016004 (2013).
5. M. Moriche, E. Hernández-Hurtado, O. Flores, M. García-Villalba, Numerical simulation of the flow around a flapping-wing micro air vehicle in free flight. *Proc. Inst. Mech. Eng. Part G J. Aerosp. Eng.*, (2018).
6. M. Keennon, K. Klingebiel, H. Won, Development of the nano hummingbird: A tailless flapping wing micro air vehicle, in *50th AIAA Aerospace Sciences Meeting including the New Horizons Forum and Aerospace Exposition* (American Institute of Aeronautics and Astronautics, 2012), pp. 1–24.
7. D. Coleman, M. Benedict, V. Hrishikeshavan, I. Chopra, Design, development and flight-testing of a robotic hummingbird. *Annu. Forum Proc. - AHS Int.* **1**, 132–149 (2015).
8. A. Roshanbin, H. Altartouri, M. Karásek, A. Preumont, COLIBRI: A hovering flapping twin-wing robot. *Int. J. Micro Air Veh.* **9**, 270–282 (2017).
9. Q.-V. Nguyen, W. L. Chan, M. Debiasi, Hybrid design and performance tests of a hovering insect-inspired flapping-wing micro aerial vehicle. *J. Bionic Eng.* **13**, 235–248 (2016).
10. H. V. Phan, T. Kang, H. C. Park, Design and stable flight of a 21 g insect-like tailless flapping wing micro air vehicle with angular rates feedback control. *Bioinspir. Biomim.* **12**, 036006 (2017).
11. C. P. Ellington, C. van den Berg, A. P. Willmott, A. L. R. Thomas, Leading-edge vortices in insect flight. *Nature* **384**, 626–630 (1996).
12. R. J. Wood, The first takeoff of a biologically inspired at-scale robotic insect. *IEEE Trans. Robot.* **24**, 341–347 (2008).
13. C. Cao, S. Burgess, A. T. Conn, Toward a dielectric elastomer resonator driven flapping wing micro air vehicle. *Front. Robot. AI* **5**, 1–11 (2019).
14. Y. Chen, H. Zhao, J. Mao, P. Chirarattananon, E. F. Helbling, N. P. Hyun, D. R. Clarke, R. J. Wood, Controlled flight of a microrobot powered by soft artificial muscles. *Nature* **575**, 324–329 (2019).
15. M. Taghavi, T. Helps, J. Rossiter, Electro-ribbon actuators and electro-origami robots. *Sci. Robot.* **3**, eaau9795 (2018).
16. Z. Suo, Theory of dielectric elastomers. *Acta Mech. Solida Sin.* **23**, 549–578 (2010).
17. H. A. Pohl, The motion and precipitation of suspensoids in divergent electric fields. *J. Appl. Phys.* **22**, 869–871 (1951).
18. H. Pellat, Électrostatique non fondée sur les lois de coulomb. Forces agissant sur les diélectriques non électrisés. Forces agissant sur les diélectriques non électrisés. *J. Phys. Théorique Appliquée* **5**, 244–256 (1896).
19. M. Dickinson, J. Lighton, Muscle efficiency and elastic storage in the flight motor of drosophila. *Science* **268**, 87–90 (1995).
20. C. A. de Saint-Aubin, S. Rosset, S. Schlatter, H. Shea, High-cycle electromechanical aging of dielectric elastomer actuators with carbon-based electrodes. *Smart Mater. Struct.* **27**, 074002 (2018).
21. J. D. W. Madden, N. A. Vandesteeg, P. A. Anquetil, P. G. A. Madden, A. Takshi, R. Z. Pytel, S. R. Lafontaine, P. A. Wieringa, I. W. Hunter, Artificial muscle technology: Physical principles and naval prospects. *IEEE J. Ocean. Eng.* **29**, 706–728 (2004).
22. F. O. Lehmann, M. H. Dickinson, The changes in power requirements and muscle efficiency during elevated force production in the fruit fly Drosophila melanogaster. *J. Exp. Biol.* **200**, 1133–1143 (1997).
23. M. S. Tu, Submaximal power output from the dorsolongitudinal flight muscles of the hawkmoth manduca sexta. *J. Exp. Biol.* **207**, 4651–4662 (2004).
24. Z. Liu, X. Yan, M. Qi, X. Zhang, L. Lin, Low-voltage electromagnetic actuators for flapping-wing micro aerial vehicles. *Sens. Actuators A Phys.* **265**, 1–9 (2017).
25. R. B. Bramlette, R. M. Barrett-Gonzalez, Design and flight testing of a convertible quadcopter for maximum flight speed, in *55th AIAA Aerospace Sciences Meeting* (American Institute of Aeronautics and Astronautics, 2017), pp. 1–19.
26. V. Hrishikeshavan, J. Black, I. Chopra, Design and performance of a quad-shrouded rotor Micro air vehicle. *J. Aircr.* **51**, 779–791 (2014).
27. Y. Nan, M. Karásek, M. E. Lalami, A. Preumont, Experimental optimization of wing shape for a hummingbird-like flapping wing micro air vehicle. *Bioinspir. Biomim.* **12**, 026010 (2017).
28. K. Y. Ma, P. Chirarattananon, S. B. Fuller, R. J. Wood, Controlled flight of a biologically inspired, insect-scale robot. *Science* **340**, 603–607 (2013).
29. Z. Liu, X. Yan, M. Qi, D. Huang, X. Zhang, L. Lin, Electrostatic flapping-wing actuator with improved lift force by the pivot-spar bracket design. *Sens. Actuators A Phys.* **280**, 295–302 (2018).
30. J. H. Marden, M. G. Kramer, Surface-skimming stoneflies: A possible intermediate stage in insect flight evolution. *Science* **266**, 427–430 (1994).
31. X. Ji, X. Liu, V. Cacucciolo, M. Imboden, Y. Civet, A. El Haitami, S. Cantin, Y. Perriard, H. Shea, An autonomous untethered fast soft robotic insect driven by low-voltage dielectric elastomer actuators. *Sci. Robot.* **4**, eaaz6451 (2019).
32. H. Wagner, M. Weger, M. Klaas, W. Schröder, Features of owl wings that promote silent flight. *Interface Focus* **7**, 20160078 (2017).
33. N. T. Jafferis, E. F. Helbling, M. Karpelson, R. J. Wood, Untethered flight of an insect-sized flapping-wing microscale aerial vehicle. *Nature* **570**, 491–495 (2019).
34. E. Leroy, R. Hinchet, H. Shea, Multimode hydraulically amplified electrostatic actuators for wearable haptics. *Adv. Mater.* **32**, 2002564 (2020).
35. S. Pourazadi, A. Shagerdmootaab, H. Chan, M. Moallem, C. Menon, On the electrical safety of dielectric elastomer actuators in proximity to the human body. *Smart Mater. Struct.* **26**, 115007 (2017).
36. G. C. H. E. de Croon, M. A. Groen, C. De Wagter, B. Remes, R. Ruijsink, B. W. van Oudheusden, Design, aerodynamics and autonomy of the DelFly. *Bioinspir. Biomim.* **7**, 025003 (2012).
37. B. H. Cheaw, H. W. Ho, E. Abu Bakar, Wing design, fabrication, and analysis for an x-wing flapping-wing micro air vehicle. *Drones* **3**, 65 (2019).
38. K. Warfvinge, L. Christoffer Johansson, A. Hedenström, Hovering flight in hummingbird hawkmoths: Kinematics, wake dynamics and aerodynamic power. *J. Exp. Biol.* **224**, 230920 (2021).

Acknowledgments: LAZA animation was provided by Elastic Pie Films. **Funding:** T.H. was supported by the Royal Academy of Engineering and the Office of the Chief Science Adviser for National Security under the UK Intelligence Community Postdoctoral Fellowship Programme and the Engineering and Physical Sciences Research Council (EPSRC) through grant EP/M020460/1. C.R. was supported by the Secretariat of Higher Education, Science, Technology and Innovation (Senescyt)—Government of Ecuador and EPSRC grant EP/M020460/1. M.T. was supported by EPSRC grant EP/R02961X/1. A.T.C. was supported by EPSRC grant EP/R02961X/1. J.R. was supported by EPSRC grants EP/M020460/1, EP/R02961X/1, EP/T020792/1, EP/V026518/1, and EP/S026096/1; the Royal Academy of Engineering through the Chair in Emerging Technologies scheme; and Royal Society—ERA Foundation Translation Award TA\R1\170060. **Author contributions:** T.H. developed the LAZA and designed experiments, with support from C.R., M.T., A.T.C., and J.R. T.H. and C.R. manufactured devices, collected data and video footage, and performed analysis. T.H. interpreted results, wrote the manuscript, and created the figures and movies. All authors reviewed and edited the manuscript. M.T., A.T.C., and J.R. advised on the project. **Competing interests:** Two patent applications have been filed relating to this work by the University of Bristol: GB1710400.1A and WO2019002860A1 (inventors: T.H., M.T., and J.R.). The other authors declare that they have no competing interests. **Data and materials availability:** All data needed to evaluate the conclusions in the paper are present in the paper or in the Supplementary Materials.

Submitted 1 April 2021
Accepted 11 January 2022
Published 2 February 2022
10.1126/scirobotics.abi8189

Science Robotics

Liquid-amplified zipping actuators for micro-air vehicles with transmission-free flapping

Tim HelpsChristian RomeroMajid TaghaviAndrew T. ConnJonathan Rossiter

Sci. Robot., 7 (63), eabi8189. • DOI: 10.1126/scirobotics.abi8189

Science Robotics (ISSN) is published by the American Association for the Advancement of Science. 1200 New York Avenue NW, Washington, DC 20005. The title *Science Robotics* is a registered trademark of AAAS.